ADVANCED MATERIALS INTERFACES

Supporting Information

for *Adv. Mater. Interfaces,* DOI: 10.1002/admi.201800802

Superfast Liquid Transfer Strategy Through Sliding on a Liquid Membrane Inspired from Scorpion Setae

Daobing Chen, Shichao Niu, Junqiu Zhang, Zhengzhi Mu, Huwei Chen, Deyuan Zhang, Zhongwen Yao, Zhiwu Han,* and Luquan Ren*

Supporting Information

Superfast liquid transfer strategy through sliding on a liquid membrane inspired from scorpion setae

Daobing Chen, Shichao Niu, Junqiu Zhang, Zhengzhi Mu, Huwei Chen, Deyuan Zhang, Zhongwen Yao, Zhiwu Han* & Luquan Ren*

Dr. D. B. Chen, Dr. S. C. Niu, Dr. J. Q. Zhang, Dr. Z. Z. Mu, Prof. Z. W. Yao, Prof. Z. W. Han, Prof. L. Q. Ren
Key Laboratory of Bionic Engineering, Ministry of Education, Jilin University, Changchun 130022, P. R. China
E-mail: niushichao@jlu.edu.cn, zwhan@jlu.edu.cn
Prof. H. W. Chen, D. Y. Zhang
School of Mechanical Engineering and Automation, Beihang University, Beijing 100191, China
Dr. J. Q. Zhang
Department of Mechanical Engineering, Columbia University, New York 10027, United States
Dr. Z. Z. Mu
Department of Chemical Engineering, University of Michigan, Ann Arbor, Michigan 48109, United States
Prof. Z. W. Yao
Department of Mechanical and Materials Engineering, Queen's University, Kingston, K7L 3N6, Canada

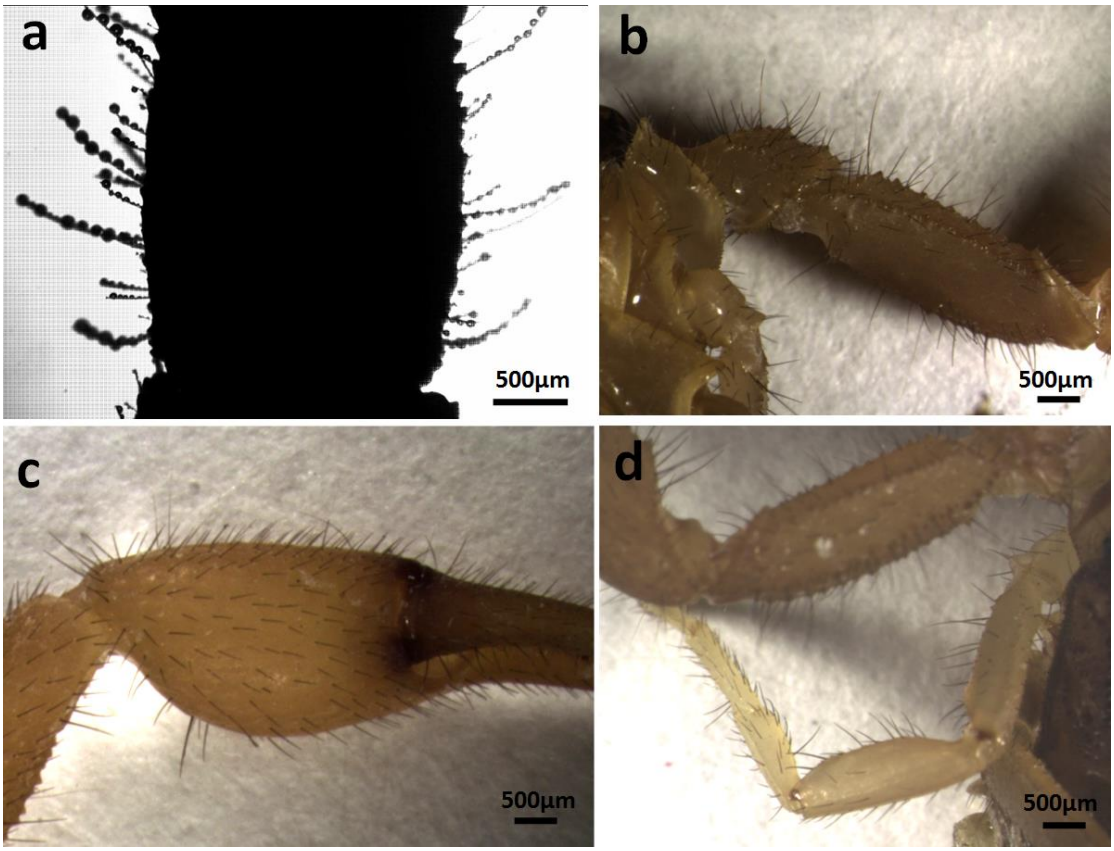

Figure S1. Optical images of the setae on a desert scorpion (*Parabuthus transvaalicus*) located on different part. (a) Image of the water captured from the fog on the tail setae of a desert scorpion. The setae are extensively distributed on its pincers (**b**) (**c**) and legs (**d**). There are a bit of setae distributed on the scorpion's back and chest. Many of setae distribute on the pectines. They all grow as a vertical needle-like array on the scorpion surface with a distances ranging from ~100 μm to 500 μm. The setae range from ~800 μm to 1300 μm in length and ~10 μm to 25 μm in diameter.

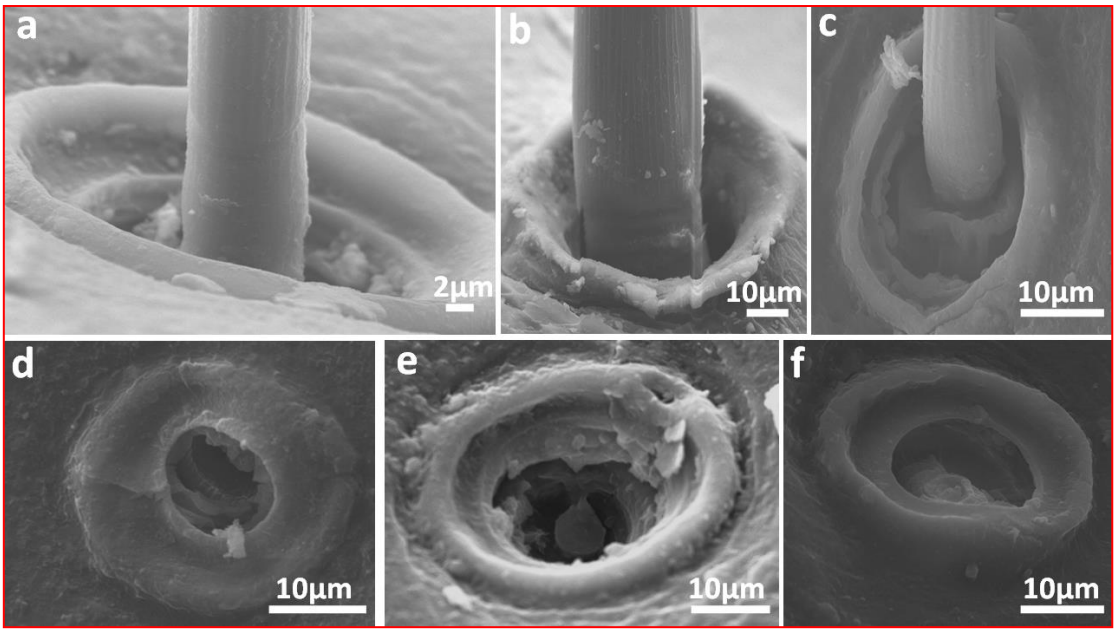

Figure S2. The sockets structure on a desert scorpion. (a-c) Sockets with seta inside. **(d-f)** Sockets without seta inside. The diameter of the sockets is larger than that of the seta. The sockets are composed of two oval circles. The inner oval circle connects the seta base with a kind of joint membrane.

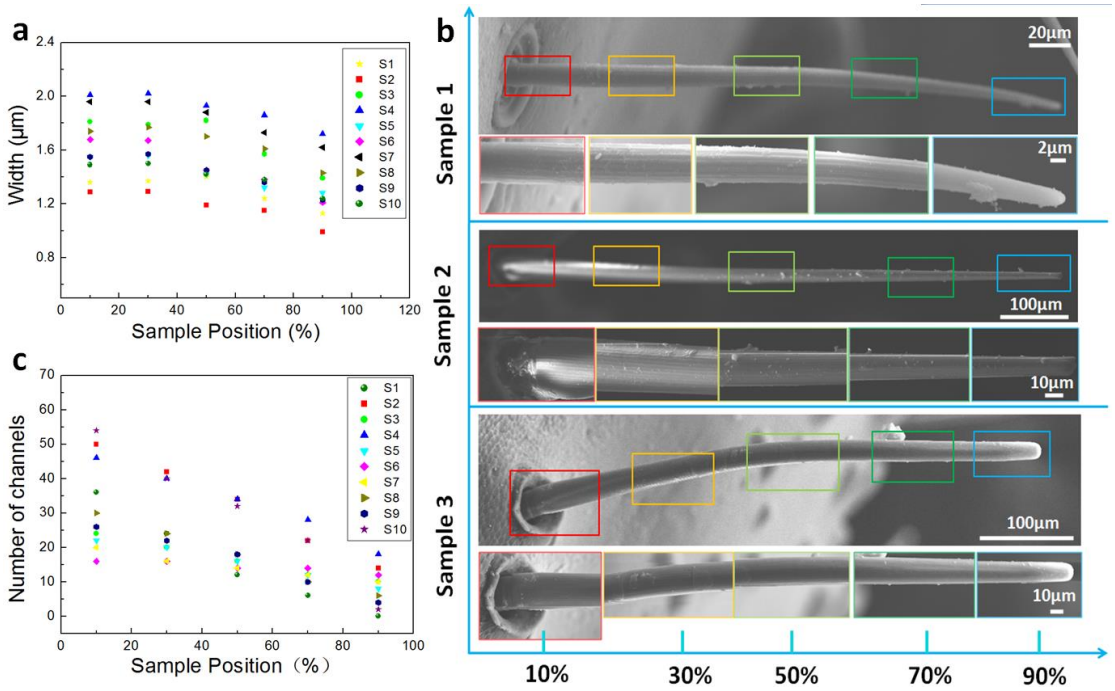

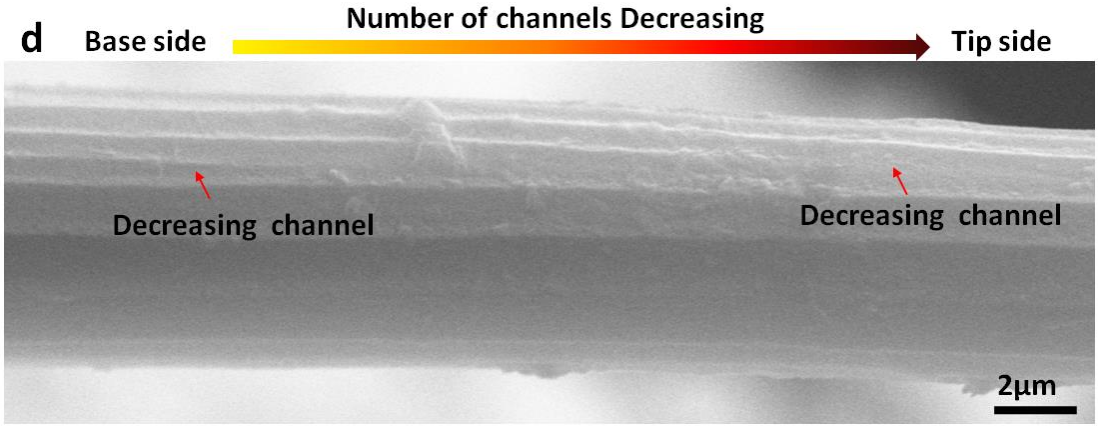

Figure S3. **Statistical measurements of the width and number of channels along the seta shaft on a desert scorpion. (a)** Ten setae were selected randomly. For each seta, the average width of the micro channels at 10%, 30%, 50%, 70% and 90% position of the entire seta length away from the base were measured. From the region near the base to the region near the tip (10% to 90%), the width of these micro channels decreased from 2 μm to 0.5 μm. **(b**) SEM images of three representative setae (Sample 1, Sample 2 and Sample 3) illustrate the gradient changes of the micro channels along the seta shaft. For each seta, the lower five images correspond with the five regions (10%, 30%, 50%, 70% and 90% of the entire seta shaft length away from the base) on the upper single seta. The micro channels near the base are dense than those near the tip. (**c)** Ten setae were selected randomly, for each seta, the numbers of micro channels at 10%, 30%, 50%, 70% and 90% position of the entire seta length away from the base were measured. From the region near the base to the region near the tip (10% to 90%), the number of these micro channels decreased. (**d)** Some channels merged with the decreasing of the radius of the seta. The red arrows point to the decreasing channel.

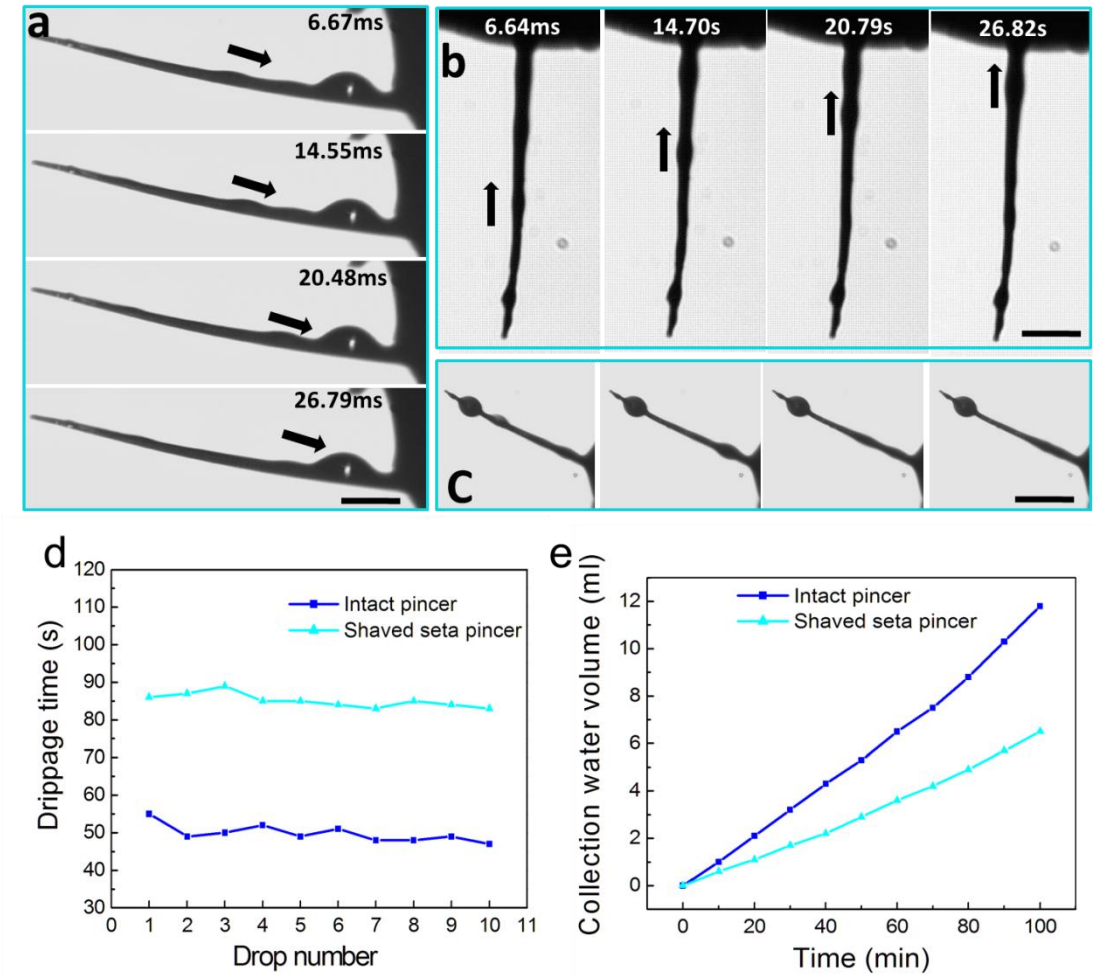

Figure S4. ***In situ*** **optical microscopic observation of the liquid-membrane water transport of different seta placed with different angles.** (**a**) Water droplet sliding mode on the liquid-membrane formed on the slightly tilted seta. (**b**) Water droplet sliding mode on the liquid-membrane formed on a vertical downwards seta. (**c**) Water droplet sliding mode on the liquid-membrane formed on a 45° tilted seta. Scale bars, 100 μm. (d, e) It can be seen, by comparing the fog collecting efficiency of the legs of scorpions with or without aetae, that there are 1 water drop produced mean interval of 50 seconds. The fog-water harvesting volume per minutes is about 0.1 mL. In contrast, the leg without setae would take much time and have a significantly lower collection efficiency.

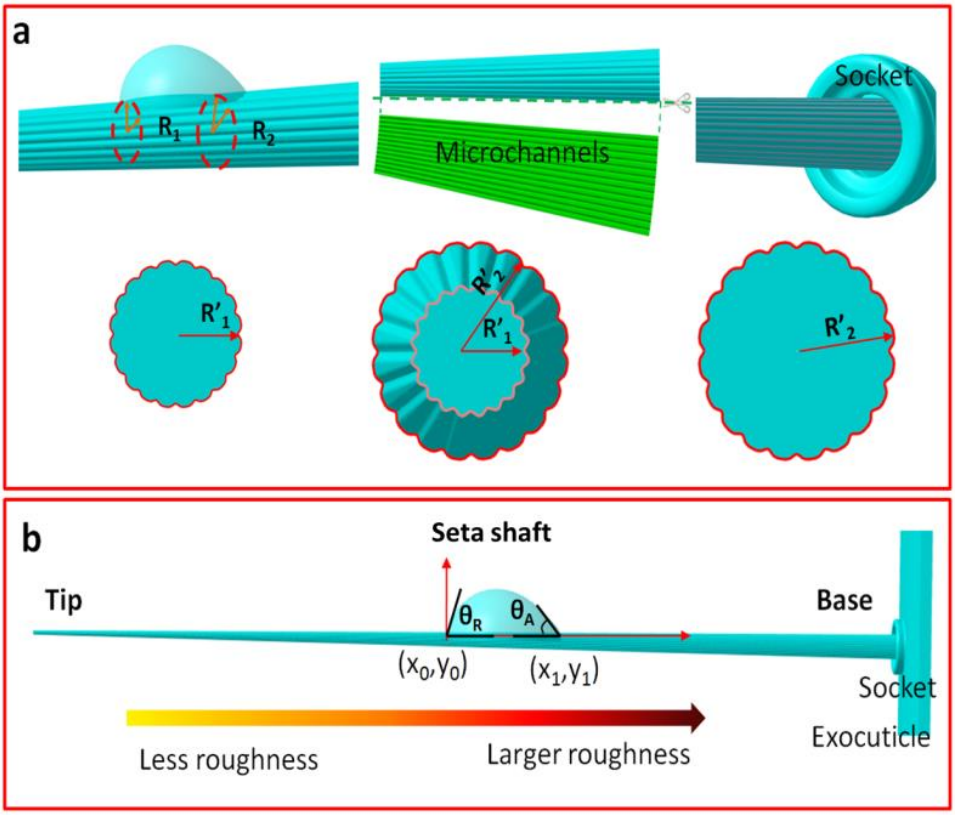

Figure S5. The difference of Laplace pressure ($\Delta P_{curvature}$) and the gradient interfacial tension (F_R) of the seta. (**a**) The conical shape of the seta generates a curvature difference ($\gamma(\frac{1}{R_1}-\frac{1}{R_2})$) from the head to the tail of water droplet. The micro gradient channels (gradient number and gradient width) would also further increase this curvature difference ($\gamma(\frac{1}{R_1'}-\frac{1}{R_2'})$). (**b**) The gradient micro channels along the seta generate a gradient surface-energy. The gradient surface-energy generates a gradient interfacial tension (F_R) along the seta. The boundary layer water is mainly driven by the gradient interfacial tension (F_R). R_1 and R_2 are the local radii of the seta shaft at the two opposite sides of the droplet. γ is the surface tension of water, R'_1 and R'_2 are the increased local radii of the seta shaft at the two opposite sides of the droplet. (x_0, y_0) is the tail point of a droplet on the seta shaft. (x_1, y_1) is the head point of a droplet on the seta shaft.

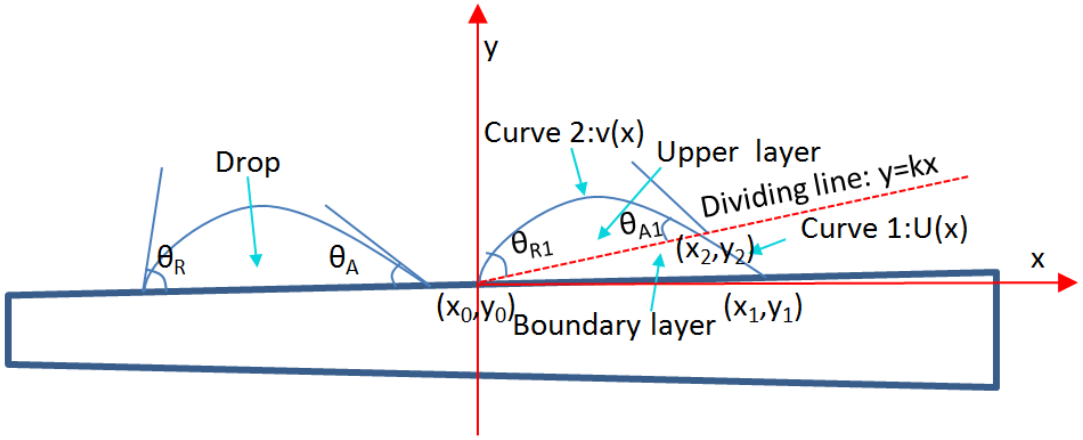

Figure S6. The droplets on the roughness surface can be divided into two layers. θ_A and θ_R are the advancing and receding contact angles of water droplets. (x_2, y_2) is the dividing point. $u(x)$ is the gas-liquid contact line under the dividing line. $v(x)$ is the gas-liquid contact line upper the dividing line. For the upper layer, the advancing angle and receding angle are same ($\theta_{R1} = \theta_{A1}$) on the dividing line. So, the advancing angle and receding angle are not same below the dividing line, generating a gradient surface-energy. Then, the droplet on the seta surface could be moved by this gradient liquid-solid interfacial tension.

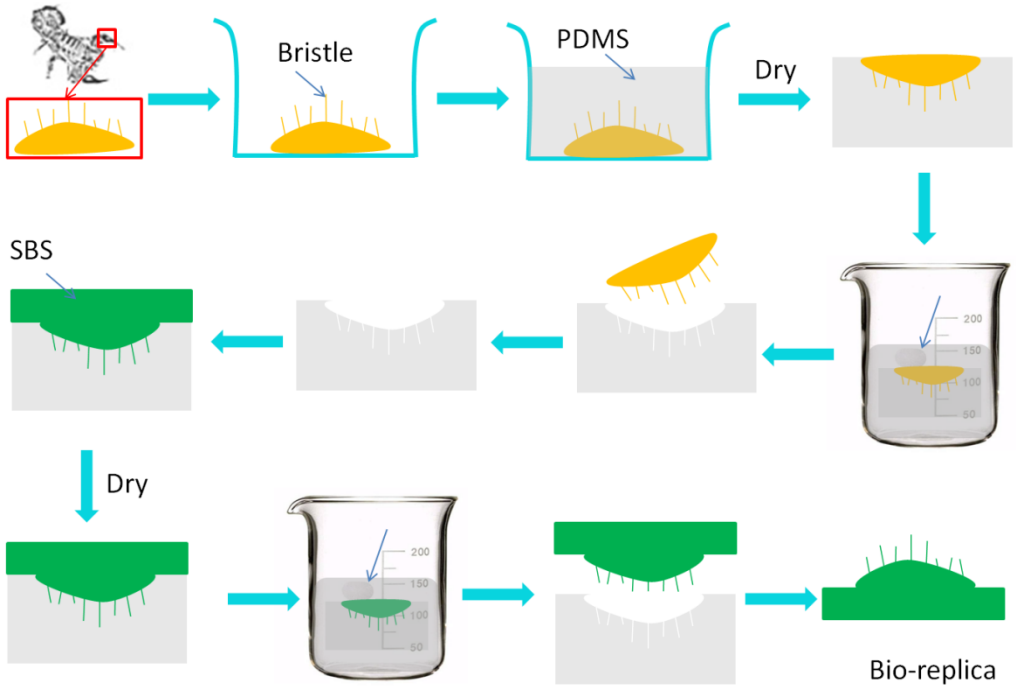

Figure S7. The fabrication schedule of the artificial seta. A simple twice bio-template method is used to fabricate the artificial seta using polydimethylsiloxane (PDMS) and

styreneic block copolymer (SBS). SEM images (Figure S9) show that all of the surface shape and structure features of the seta were accurately transferred from the original setae on the desert scorpion to the artificial replicas. (For detailed process of sample preparation and fabrication, see References below)

References

[1] M. H. Sun, C. X. Luo, L. P. Xu, H. Ji, O. Y. Qi, D. P. Yu, Y. Chen, *Langmuir* **2005**, *21*, 8978.

[2] H. W. Chen, P. F. Zhang, L. W. Zhang, H. L. L. Iu, Y. Jiang, D. Y. Zhang, Z. W. Han, L. Jiang, *Nature* **2016**, *532*, 85.

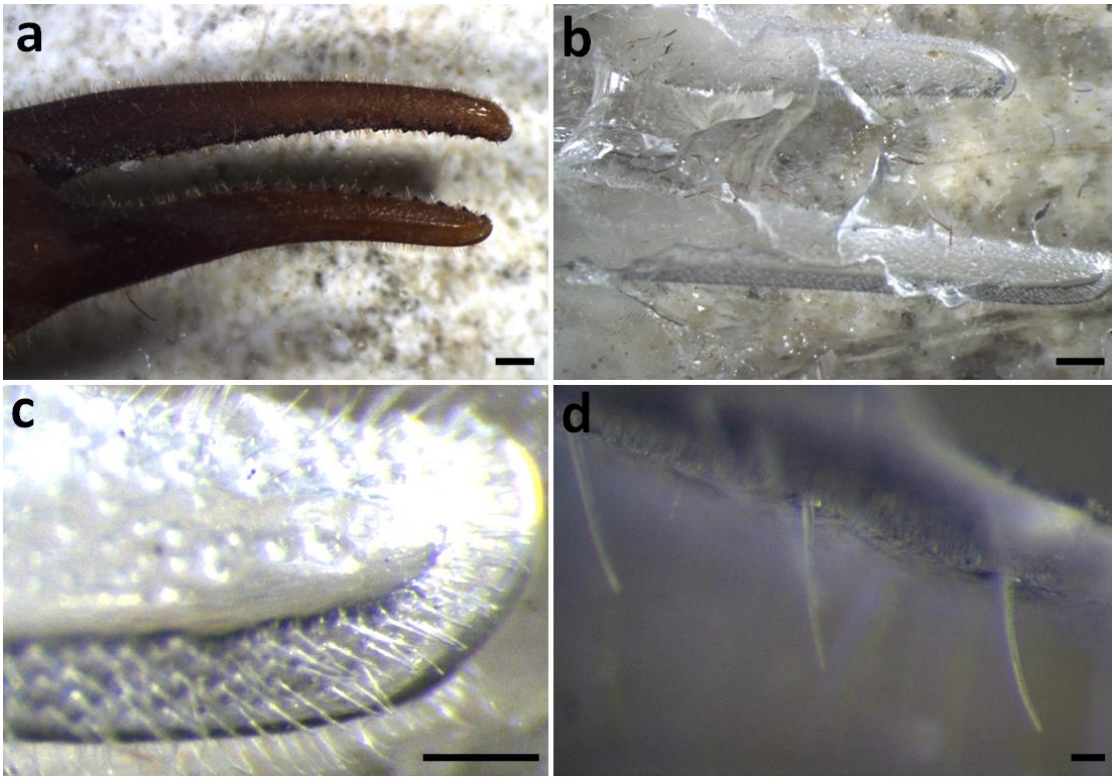

Figure S8. The images of the artificial replica setae. (**a**) The natural scorpion pincer. (**b**), (**c**) and (**d**) Images of the artificial seta. It can be seen from (b) that the macro profile of scorpion legs has been successfully replicated. Remarkably, the setae are also replicated on its legs surface, which can be confirmed by (c). Also, the single seta is also clearly replicated form (d).

Scale bars, 500 μm (**a**), 500 μm (**b),** 200 μm **(c),** 20 μm **(d**)

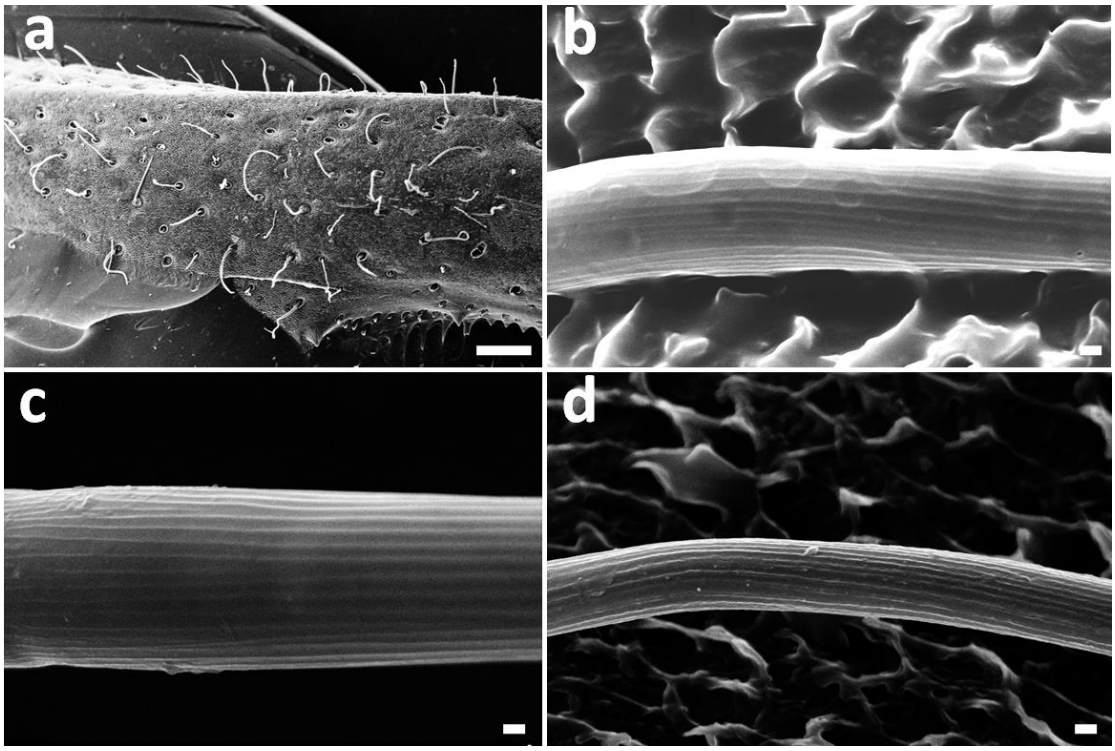

Figure S9. SEM images of the artificial setae. (a) SEM image of the scorpion leg surface. There are several setae on its surface, which is replicated from the original desert scorpion. (b-d) SEM images of the single seta surface. It can be confirmed that there are micro grooves on the seta surface, which are also replicated from the scorpion setae. Based on the results above, it can be confirmed that not only the shapes of the seta but also its surface structures are all replicated down from the original setae of the desert scorpion. Besides, the fast sliding movement of the droplets on the liquid membrane on the seta surface is also replicated successfully, which can be confirmed from the Movie S4. Scale bars, 200 μm (**a**), 2 μm (**b),** 2 μm **(c),** 2 μm **(d**).

Theory S1:

When a droplet move on a conical-shaped surface, it is often driven toward the side with the larger radius due to the difference of the Laplace pressure[1]. As illustrated in Figure 4b, a

single seta on a desert scorpion can be considered as a conical object with linear channels (see Figure S5a). This conical shape generates difference of Laplace pressure ($\Delta P_{\text{curvature}}$) between the two opposite sides of the droplet as follows[2]:

$$\Delta P_{curvature} = -\int_{R_1}^{R_2} \frac{2\gamma}{(R+R_0)^2} \sin\alpha dz \qquad (1)$$

where R is the local radius of the seta shaft, R_1 and R_2 are the local radii of the seta shaft at the two opposite sides of the droplet, γ is the surface tension of water, R_0 is the droplet radius, α is the half-apex angle of the conical seta, and dz is the incremental radius of the seat. The Laplace pressure on the tip region of the seta (small radius R_1) is larger than that near the base (large radius R_2). This difference ($\Delta P_{\text{curvature}}$) within the water droplet initiates a driving force that makes the droplet move from the tip side to the base side along the seta shaft.

The micro channels and ridges on the seta surface have a gradient number and gradient width. The channels are sparser near the tip (less rough) than near the base (rougher) of the seta (Figure S5b). This roughness can be described using Wenzel's equation [3] as follows:

$$\cos\theta_w = \gamma \cdot \cos\theta \qquad (2)$$

Where r is the roughness factor defined as the ratio of the actual surface area to the geometric projected area of a rough surface, and θ and θ_w are the intrinsic and apparent contact angles, respectively. The gradient of roughness generates a gradient of wettability, (that is, a gradient of surface-free energy). For surface of the seta, the base is rougher and more hydrophilic; whereas the tip is less rough and less hydrophilic (see Figure S5b). In other words, the tip of the seta has a lower surface-free energy than the base. This gradient of the surface-free energy produces a driving force(*F),* driving the water droplets captured on the tip directionally towards the base as described as follows[4]:

$$F_R = \int_{x_0}^{x_1} \gamma(\cos\theta_A - \cos\theta_R) dl \qquad (3)$$

Where θ_A and θ_R are the advancing and receding contact angles of water droplets on the middle of the seta, respectively, and dl is the integral variable along the length of the droplet

from the tail (x_0) to the head (x_1). The roughness arisen from the microgrooves on the seta enhances the difference of Laplace pressure (see Figure S5a), contributing to the movement of the water droplets along the seta.

Theory S2:

Since the concept of modern fluid mechanics was first proposed, the boundary layer has become an important topic in the field of fluid mechanics. The boundary layer is a thin layer. It cannot be ignored by the viscous force of the high Reynolds number flow around the material surface. The water droplets driven by the gradient roughness and shape gradients can be also analyzed by the boundary layer theory[5]. For the traditional fluid mechanics, fluid velocity of the upper layer is faster than that of the boundary layer. However, the situation is just the opposite. The velocity of the droplet was determined by the wetting velocity. As shown in Figure S6, the moving droplet on the seta was separated into upper layer and boundary layer. The boundary layer water thickness (δ_1) can be expressed as:

$$\delta_1 = \int_0^{x_2} kxdx + \int_{x_1}^{x_2} u(x)dx \qquad (4)$$

The upper layer water thickness (δ_2) can be expressed as:

$$\delta_2 = \int_0^{x_2} (v(x) - kx)dx \qquad (5)$$

Where x_2 is the dividing point, x_1 is the advancing contact point, $u(x)$ is the boundary layer water contact line, $v(x)$ is the upper layer water contact line, and dx is the incremental distance from the O (x_0, y_0) point.

References:

[1] L. E, Q. D, *Journal of Fluid Mechanics* **2004**, *510*, 29.

[2] J. Ju, H. Bai, Y. Zheng, T. Zhao, R. Fang, L. Jiang, *Nature Communications* **2012**, *3*, 1247.

[3] R. N. Wenzel, *Ind.eng.chem* **1936**, *28*, 988.

[4] H. Bai, X. Tian, Y. Zheng, J. Ju, Y. Zhao, L. Jiang, *Advanced Materials* **2010**, *22*, 5521.

[5] H. W. Chen, P. F. Zhang, L. W. Zhang, H. L. L. Iu, Y. Jiang, D. Y. Zhang, Z. W. Han, L. Jiang, *Nature* **2016**, *532*, 85.

Movies:

Movie S1: Fog capture process in real-time of a single seta placed vertical to the ground. The water droplets can transport from the tip side to the base side of the seta shaft. The water droplet transport mode changed from the crawl mode to the sliding mode on the fast sequence liquid membrane.

Movie S2: Further enlarged movie reveal the details of the sliding mode on the fast sequence liquid membrane. The movie was recorded at 4000 fps by the high-speed cameras (PCO. dimax HD, Germany). The play rate of the movie was 100 fps.

Movie S3: After the liquid membrane formed on surface of the seta, a single seta was placed in thin fog environment. It still has the ability of capturing fog and transporting water droplet fast and efficiently in the sliding mode.

Movie S4: Fog capture process of the artificial seta that placed vertical to the ground. The water drops can transport from the tip side to the base of the replica. Also, the liquid membrane can also be formed on the surface of the artificial seta. In summary, the fast sliding movement of the droplets on the liquid membrane of the seta surface is also replicated successfully.